RSC Advances

PAPER

View Article Online
View Journal | View Issue

Cite this: *RSC Adv.*, 2020, **10**, 13759

Application of temperature-controlled chiral hybrid structures constructed from copper(II)-monosubstituted Keggin polyoxoanions and copper(II)-organoamine complexes in enantioselective sensing of tartaric acid†

Mu-Xiu Yang, Meng-Jie Zhou, Jia-Peng Cao, Ye-Min Han, Ya-Lin Hong and Yan Xu *

Temperature usually occupies a crucial position in the construction of chiral compounds. By controlling the temperature of the reaction system, chiral and non-chiral compounds can be designed and synthesized. Given the above, three new chiral and non-chiral compounds based on copper(II) monosubstituted polyoxoanions and Cu(en) complexes (en = ethylenediamine), D/L-$[Cu(H_2O)(en)_2]_2\{[Cu(H_2O)_2(en)][SiCuW_{11}O_{39}]\}\cdot 5H_2O$ (**1**, D-**1** and L-**1**) and $[Cu(H_2O)(en)_2]\{[Cu(en)_2]_2[SiCuW_{11}O_{39}]\}\cdot 2.5H_2O$ (**2**), were successfully synthesized under hydrothermal conditions. The main synthesis conditions of compound **1** (D-**1** and L-**1**) and compound **2** are the same, however, the only difference is that the reaction temperatures are 80 °C and 140 °C, respectively. What's more, compounds **1** and **2** can form a 1D chiral chain by Cu–O and W/Cu–O–W/Cu bonds, respectively, and further obtain a 3D-supramolecular framework through hydrogen bonding interaction. Meanwhile, due to the asymmetry of chiral compound **1**, optical second-harmonic generation (SHG) was used to investigate the second-order nonlinear optical effect and it was found that the observed SHG efficiency of compound **1** is 0.3 times that of urea. To further investigate the chiral properties, D-**1** and L-**1** were used in the electrochemical enantioselective sensing of D-/L-tartaric acid (D-/L-tart) molecules, respectively, which demonstrates that D-**1** and L-**1** have a good application prospect in sensing chiral substances.

Received 28th February 2020
Accepted 25th March 2020

DOI: 10.1039/d0ra01904f

rsc.li/rsc-advances

Introduction

Polyoxometalates (POMs), one of the most significant metal–oxygen cluster materials, have raised many concerns because of their structural variability and potential applications in many fields of nonlinear optics,[1] catalysis,[2] magnetism,[3] materials science,[4] luminescence,[5] *etc.*

Chiral polyoxometalates (CPOMs), as a special subclass of POMs, contain intriguing architectures, and are a good research prospect.[6] As the previous reported literature,[7] chiral POM-based frameworks can be approached *via* two synthetic strategies. The first method can be realized by the use of enantiomerically pure chiral inducement, including chiral metal–organic fragments and organic ligands.[8] The second tactic is using achiral precursors *via* spontaneous resolution to yield a polymer consisting of a pair of enantiomers, while the entire polymer is racemic.[9] Notably, most efforts so far have been made to explore the first method, while the second method has rarely been developed. Although many groups have committed to synthesize chiral POMs through spontaneous resolution, and the studies of achiral structures to chiral structures in metal–organic frameworks (MOFs) have developed rapidly in the last few decades,[10] limited examples of POMs in such aspects have been reported.[11] The information associated with the key factors which dominates the construction of chiral and achiral compounds has also been uncommonly reported until now. Moreover, spontaneous resolution cannot be predicted in advance since the laws of physics which determines the process outputs have not been completely understood. Although there are many examples of chiral MOFs[12] as well as their spontaneous resolution,[13] it is more difficult to design and build chiral POM-based compounds. The data show that merely 5–10% racemates can become the conglomerate, indicating that spontaneous resolution of achiral components in chiral POM chemistry is a great challenge.[14]

To the best of our knowledge, temperature usually occupies a crucial position in the construction of POMs. Furthermore, by

College of Chemical Engineering, State Key Laboratory of Materials-Oriented Chemical Engineering, Nanjing Tech University, Nanjing 210009, P. R. China. E-mail: yanxu@njtech.edu.cn

† Electronic supplementary information (ESI) available: TG curves, IR spectra, PXRD patterns, nonlinear optical measurement. CCDC 1837268–1837270 for compounds **1–2**. For ESI and crystallographic data in CIF or other electronic format see DOI: 10.1039/d0ra01904f

Table 1 Crystal data and structure refinements for **1–2**

Compound	D-**1**	L-**1**	**2**
Formula	$C_{10}H_{58}N_{10}O_{48}SiW_{11}Cu_4$	$C_{10}H_{58}N_{10}O_{48}SiW_{11}Cu_4$	$C_{12}H_{55}N_{12}O_{42.5}SiW_{11}Cu_4$
Formula weight	3391.26	3391.26	3352.28
Crystal system	Triclinic	Triclinic	Monoclinic
Space group	*P*1	*P*1	*P*2(1)/*c*
a (Å)	10.970(4)	10.9871(11)	18.900(5)
b (Å)	12.408(4)	12.3354(12)	23.208(6)
c (Å)	12.818(4)	12.7954(13)	26.175(7)
α (deg.)	101.383(4)	101.8070(10)	90
β (deg.)	111.028(4)	110.3310(10)	96.397(3)
γ (deg.)	108.089(4)	107.7180(10)	90
V (Å^3)	1451.3(8)	1452.5(3)	11 410(5)
Z	1	1	8
D_c (mg m^{-3})	3.880	3.877	3.903
F (000)	1516	1516	11 960
Crystal size (mm^3)	0.120 × 0.100 × 0.100	0.130 × 0.110 × 0.100	0.150 × 0.130 × 0.120
Limiting indices	$-13 \le h \le 12$, $-14 \le k \le 14$, $-12 \le l \le 15$	$-13 \le h \le 12$, $-14 \le k \le 14$, $-15 \le l \le 15$	$-22 \le h \le 22$, $-27 \le k \le 27$, $-31 \le l \le 31$
Reflections collected/ unique	10 382/8081	10 722/8269	79 061/20 131
R(int)	0.0478	0.0329	0.2186
Data/restraints/ parameters	8081/456/748	8269/445/757	20 131/589/1486
GOF	1.029	1.100	1.052
Absolute structure parameter	0.06(2)	0.02(2)	
R_1[a], wR_2[b] [$I > 2\sigma(I)$]	$R_1 = 0.0517$, w$R_2 = 0.1249$	$R_1 = 0.0483$, w$R_2 = 0.1304$	$R_1 = 0.0718$, w$R_2 = 0.1717$
R_1, wR_2 (all data)	$R_1 = 0.0565$, w$R_2 = 0.1356$	$R_1 = 0.0591$, w$R_2 = 0.1697$	$R_1 = 0.1031$, w$R_2 = 0.1841$

[a] $R_1 = \sum||F_o| - /F_c||/\sum|F_o|$. [b] $wR_2 = \sum[w(F_o^2 - F_c^2)^2]/\sum[w(F_o^2)^2]^{1/2}$.

adjusting the reaction temperature, chiral or non-chiral POMs compounds can be synthesized.[10a,11] Zheng's group have reported a chiral vanadium phosphonate compound, synthesising from non-chiral materials at 120 °C. Upon heating, chirality of the compound releases and leads to an achiral compound.[15] An and co-workers documented the $[Co_2Mo_{10}H_4O_{38}]^{6-}$ as a model and constructed chiral and non-chiral compounds at 85 °C and 25 °C, respectively, which is an intriguing example of chiral POMs to achiral POMs transformation.[16] In addition, the chiral POMs had good applications in catalysis, enantioselective identification, non-linear optics, *etc.*,[6,17] but the investigation of chiral POMs is still relatively limited. Thus, it is urgent to explore the property of chiral POMs.

Given the above mentioned, we designed and synthesized chiral conglomerates D- and L-$[Cu(H_2O)(en)_2]_2\{[Cu(H_2O)_2(en)][SiCuW_{11}O_{39}]\}\cdot 5H_2O$ (D-**1**, L-**1**), synthesising from achiral precursors *via* spontaneous resolution, obtaining at 80 °C. While compound $[Cu(H_2O)(en)_2]\{[Cu(en)_2]_2[SiCuW_{11}O_{39}]\}\cdot 2.5H_2O$ (**2**) was obtained at 140 °C, and the chirality disappeared, becoming an achiral compound. They represent the example of chiral compounds to achiral compounds in the area of POMs and it also manifests that the reaction temperature is a crucial factor to mediate the formation of achiral compounds and chiral compounds. The chiral POMs were obtained from achiral precursors *via* the spontaneous resolution method by controlling the temperature, which may have a certain guiding effect on the subsequent chiral POMs synthesis. In addition, electrochemical measurements demonstrate that carbon paste electrodes prepared by D- and L-**1** (D- and L-cpe) exhibited remarkable electrochemical enantioselective sensing to chiral substances (D/L-tart molecule).

Experimental section

Materials and physical measurements

$K_8[\alpha\text{-}SiW_{11}O_{39}]\cdot 13H_2O$ was prepared according to the literature,[18] while other chemicals were purchased and put to use without further purification. Elemental analyses (C, H, and N) were performed with an elemental analyzer (PerkinElmer 2400). IR spectra of compounds **1–2** were recorded on a Nicolet Impact 410 FTIR spectrometer in the range of 400–4000 cm^{-1} with pressed KBr pellets. In flowing N_2 atmosphere, thermogravimetric measurement (TG) was performed on a diamond thermogravimetric analyzer, and the test temperature increased from 25 to 700 °C at a rate of 10 °C min^{-1}. Bruker D8X diffractometer equipped with monochromatized Cu-K_α (λ = 1.5418 Å) radiation was used to record Powder X-ray diffraction (PXRD) at room temperature, and data were collected in the range of 5° to 50°. The circular dichroism spectra were obtained with the use of JASCOJ-810 spectropolarimeter.

X-ray crystallography

Bruker Apex II CCD using Mo-Kα radiation (λ = 0.71073 Å) was applied to collect the crystallographic analyses data of

compounds **1** and **2** under room temperature. In addition, the *SHELX-2014* program package was taken to resolve the crystal structures with direct methods, and F^2-based full-matrix least-squares methods were used to further refine the crystal structure. Refine the H atoms of organic molecules with specified isotropic thermal parameters, but hydrogen atoms for water were not situated. Compared with W atoms, the N, C and O atoms are very light, and not stable during refinement. The thermal parameters of some N, C and O atoms are restrained. The structural determination and crystal data for three compounds are disposed and presented in Table 1. Selected bond lengths (Å) and angles (°) and hydrogen bonds are shown in Tables S2–S4 and Tables S5–S7,† respectively.

Synthesis of compounds

D- and L-$[Cu(H_2O)(en)_2]_2\{[Cu(H_2O)_2(en)][SiCuW_{11}O_{39}]\}\cdot 5H_2O$ (1) *(D-1 and L-1).* $Cu(OAc)_2\cdot H_2O$ (0.1002 g, 0.5 mmol) and $K_8[\alpha\text{-}SiW_{11}O_{39}]\cdot 13H_2O$ (0.3012 g, 0.094 mmol) were placed into 3 ml ethanol and 6 ml CH_3COOH–CH_3COONa buffer solution and stirred for 0.5 h. Then ethylenediamine (0.0502 g 0.83 mmol) was added drop by drop to the previous mixture and continued to be stirred for about 2 hours. The mixed solution was poured into a 25 ml Teflon-lined autoclave and then put in the 80 °C oven for 7 days. After cooling to room temperature, purple plate crystals were collected by washing with distilled water (yield 47.2% based on W). Elemental anal. found (%): C, 3.55; H, 1.42; N, 4.14. Calcd (%): C, 3.54; H, 1.71; N, 4.13.

$[Cu(H_2O)(en)_2]\{[Cu(en)_2]_2[SiCuW_{11}O_{39}]\}\cdot 2.5H_2O$ (2). The preparation process of compound **2** was not much different from that of compound **1**, apart from temperature was increased to 140 °C. After cooling to room temperature, purple stick crystals were isolated by washing with distilled water (yield 41.42% based on W). Elemental anal. found (%): C, 4.31; H, 1.50; N, 5.02. Calcd (%): C, 4.30; H, 1.64; N, 4.94.

Results and discussion

Synthesis

There are many methods for synthesizing POM-based compounds, among which hydrothermal synthesis is a commonly used and effective method. The reaction process of hydrothermal synthesis is complicated and unpredictable, and the final products will be certainly influenced by plenty of factors. Typical factors include starting substances (the type of reagents, concentrations of solvents, *etc.*) and the reaction conditions (temperature, pH, time, *etc.*). In our experiment, the reaction temperature is a crucial factor of the reaction system, contributing to the synthesis of three compounds. The main synthesis conditions of compound **1** (D-**1** and L-**1**) and compound **2** are the same, apart from the reaction temperature. D-**1** and L-**1** were obtained at lower temperature 80 °C, with an increase of the temperature to 140 °C, compound **2** was formed.

The IR spectra of compounds **1–2** were measured in the range of $\nu = 4000$–$400\ cm^{-1}$ (Fig. S5 and S6†). The characteristic peaks at 790, 895 cm^{-1} (**1**) and 792, 897 cm^{-1} (**2**) for ν(W–O–W); 946 cm^{-1} (**1**) and 940 cm^{-1} (**2**) for ν(W=O); 1102 cm^{-1} (**1**) and 1033 cm^{-1} (**2**) for ν(Si–O). Additionally, in the range of 1383–1593 cm^{-1} (**1**) and 1383–1590 cm^{-1} (**2**) could be ascribed to the characteristic peaks of the ethylenediamine molecules. Whereas the broad peak at about 3449 cm^{-1} (**1**) and 3464 cm^{-1} (**2**) demonstrates the presence of water molecules. The peaks discussed above are corresponding to the result of single crystal structural analyses.

As shown in Fig. S9 and S10,† the experimental PXRD patterns of samples **1–2** had relatively good agreement with the simulated PXRD patterns, while only slight differences in intensity were observed, revealing that compounds **1** and **2** have better phase purity.

Structure of D- and L-$[Cu(H_2O)(en)_2]_2\{[Cu(H_2O)_2(en)][SiCuW_{11}O_{39}]\}\cdot 5H_2O$ (D-1 and L-1) (1)

Due to crystallographic data of compounds D-**1** and L-**1** collected from single-crystal X-ray diffractometer are almost same, and the structures of the D-**1** and L-**1** are mirror symmetrical. Hence, we just take D-**1** as an example to analyze the structure detailedly. Compound D-**1** crystallizes in the chiral triclinic crystal system with a space group *P*1. The basic unit of D-**1** contains a $\{[Cu(H_2O)_2(en)][SiCuW_{11}O_{39}]\}^{4-}$ anion (Fig. 1), two independent $[Cu(H_2O)(en)_2]^{2+}$ cations, five lattice water molecules. Four separate copper cations adopt two different types of coordination geometry patterns. Cu1 coordination cation incorporated into the defect site of the polyoxoanion $[\alpha\text{-}SiW_{11}O_{39}]^{8-}$ is six-coordinated, possessing a distorted octahedron geometry, in which five coordination oxygen atoms are derived from one O-donor $[\alpha\text{-}SiW_{11}O_{39}]^{8-}$ and the last one coordination oxygen atom from the adjacent polyoxoanion. Both Cu3 and Cu4 in the independent $[Cu(H_2O)(en)_2]^{2+}$ cation display pentacoordinate distorted square pyramid geometry, which are coordinated with four nitrogen atoms from two ethylenediamine molecules and one coordination oxygen atom from lattice water molecules. The coordination mode around Cu2 in the $[Cu(H_2O)_2(en)]^{2+}$ cation is the same as that of Cu3 and Cu4, the distinction is wherein the source of the coordination oxygen atoms, two of them are supplied by lattice water molecules and the last one is provided by the O-donor polyoxoanion (Fig. S1†). Many hybrid materials based on mono-substituted Keggin anions are achiral as well as show subtle type of disorder in the solid state. It is worth mentioning that

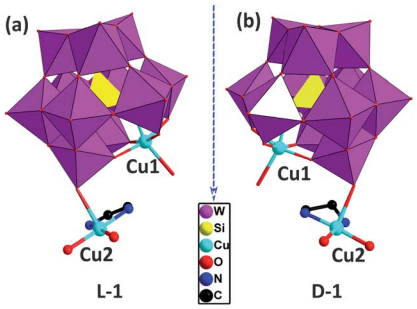

Fig. 1 The $\{[Cu(H_2O)_2(en)][SiCuW_{11}O_{39}]\}^{4-}$ anion of L-**1** (a) and D-**1** (b) (all H atoms omitted for clarity).

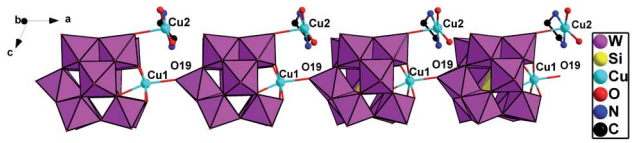

Fig. 2 Polyhedral and ball-and-stick representation of the 1D right-handed chain in D-1.

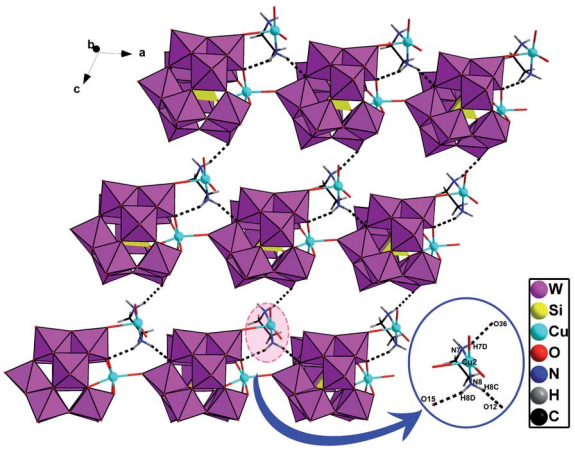

Fig. 3 The 2D homochiral sheet in D-1 (the hydrogen-bonding between the polyoxoanions and organic ligands are demonstrated).

the hybrid materials constructed from $[SiCuW_{11}O_{39}]^{6-}$ anions in this article are chiral, which is different from the previous reports. The Flack parameters (0.06(2) for D-1, 0.02(2) for L-1) and circular dichroism spectroscopy also fully demonstrate that the chiral absolute configurations of D-1 and L-1 are correct.

In D-1, chiral subunits $\{[Cu(H_2O)_2(en)][SiCuW_{11}O_{39}]\}^{4-}$ are bridged together to come into being a 1D chiral chain through Cu1–O19 (Fig. 2). The bond length of Cu1–O19 interaction in compound **1** is 2.40(2) Å. Due to the axial extension of the Jahn–Teller effect of copper(II) ions, which is considered that a usual coordination bond is formed between Cu1–O19. And the adjacent right-handed chains are joined up together by strong hydrogen bonds (N–H···O), generating a 2D supramolecular chiral layer (Fig. 3). Moreover, 2D chiral sheets are linked together through hydrogen-bonding interactions (N–H···O) to come into being a 3D supramolecular chiral network (Fig. 4). The bond lengths of Cu–O and Cu–N are in the scope of 1.950(2)–2.440(3) Å and 1.948(4)–2.055(3) Å, respectively. The valence of the Cu cations is +2, which is obtained from the bond valence sum (BVS) calculations (Table S1†). Compound **1** can be manually separated under a polarizing microscope.

Structure of $[Cu(H_2O)(en)_2]\{[Cu(en)_2]_2[SiCuW_{11}O_{39}]\}\cdot 2.5H_2O$ (2)

When adjusting the reaction temperature from 80 °C to 140 °C under the similar conditions, achiral compound **2** was obtained. Compound **2** crystallizes in the monoclinic system and space group $P2_1/c$. The asymmetric structural unit of compound **2** is occupied by a $\{[Cu(en)_2]_2[(SiW_{11}CuO_{39})]\}^{2-}$ anion, one free $[Cu(H_2O)(en)_2]^{2+}$ cation, and 2.5 lattice water molecules (Fig. 5).

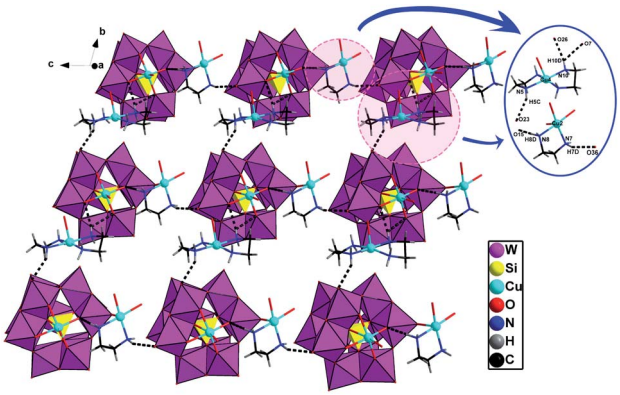

Fig. 4 The 3D supramolecular homochiral network in D-1 (the hydrogen-bonding between the polyoxoanions and organic ligands are demonstrated).

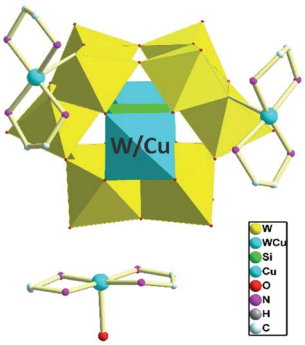

Fig. 5 Polyhedral and ball-and-stick representation of asymmetric unit in compound **2**.

Fig. 6 Polyhedral representation of the 1D chain in **2** (the dimethylamine molecules and H atoms are omitted for clarity).

The coordination environments of four Cu^{2+} cations in compound **2** are similar to that of compound **1**. In addition, Cu and W atoms in $[(SiW_{11}CuO_{39})]^{6-}$ anion are statistically disordered, occupying half of the Cu/W positions in the cluster, respectively.

As shown in Fig. 6, turning one $[(SiW_{11}CuO_{39})]^{6-}$ ion ~45° around the anionic equatorial plane and then connected the adjacent planar $[(SiW_{11}CuO_{39})]^{6-}$ ion by terminal oxygen atoms of $[(SiW_{11}CuO_{39})]^{6-}$ ion, generating a one-dimensional chain construction. The bond length and the bond angle of W/Cu–O–W/Cu were 3.7779(26) Å and 158.253(13)°, respectively. Adjacent chiral chains are interconnected by hydrogen-bonding (N–H···O) to produce a 2D supramolecular achiral layer (Fig. 7). Furthermore, these 2D sheets are further connected into 3D open framework by hydrogen bonds (Fig. 8).

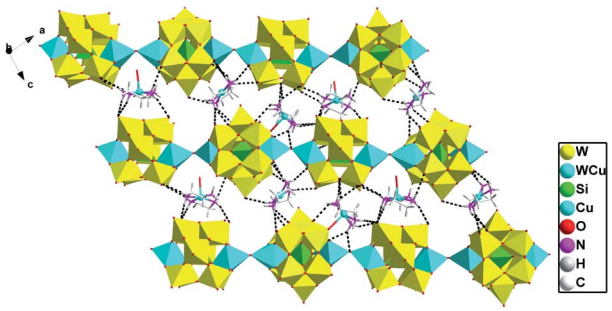

Fig. 7 2D achiral sheet in compound **2** (the hydrogen-bonding between the polyoxoanions and organic ligands are demonstrated).

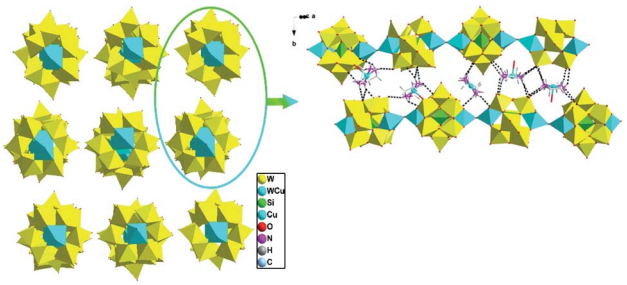

Fig. 8 View of 3D supramolecular achiral framework in **2** (all dimethylamine molecules and H atoms omitted for clarity), the hydrogen-bonding interactions between the adjacent 2D achiral sheets.

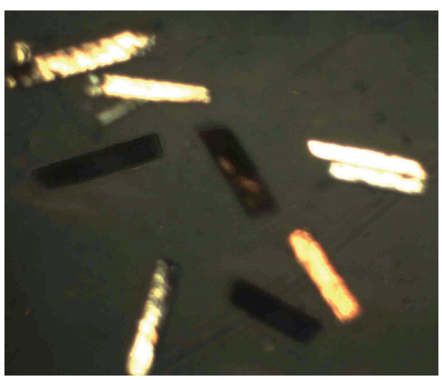

Fig. 9 The display of light D-**1** and dark L-**1** under polarizing microscope.

CD spectrum

The crystal samples of compound **1** show dark and bright forms under polarizing microscope with polarized light (Fig. 9), while their crystal colors, shapes and sizes are almost identical under normal microscopes. Therefore, D-**1** and L-**1** can be manually separated under a polarizing microscope to further measure their solid state circular dichroism (CD) spectra,[19] which is employed to further discuss the chiral optical activity of them. The CD spectra of D-**1** and L-**1** samples are symmetrical to each other (Fig. 10). Within the range of 150–700 nm, D-**1** first presented a negative Cotton effects at λ = 281 nm, and then

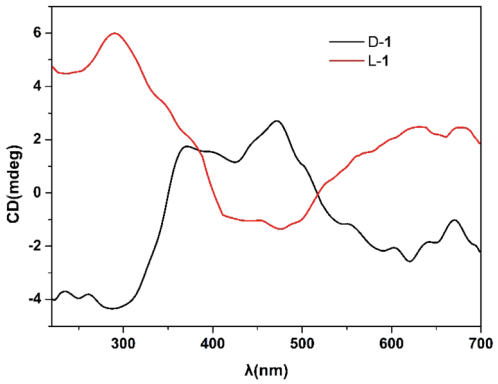

Fig. 10 CD spectra for D-**1** and L-**1**.

presented a positive Cotton effects λ = 475 nm. As expected, at the same wavelength, L-**1** exhibits the opposite cotton effects to D-**1**, demonstrating that they are enantiomers.[20]

Nonlinear optical measurement

Nonlinear optical properties belong to a research direction of chiral polyoxometalates.[17d-g] Considering the asymmetry of chiral compound **1**, optical second-harmonic generation (SHG) was used to investigate second-order nonlinear optical effect of mixed crystal samples (D-**1** and L-**1**). The SHG intensity data of compound **1** was measured on the Q-switched Nd:YAG laser (λ = 1064 nm), and microcrystalline urea was selected as standard nonlinear optical material. The result showed that the observed SHG efficiency of compound **1** is 0.3 times that of urea.

Meanwhile, third-order NLO properties of D-**1** and L-**1** were investigated by the open-aperture *Z*-scan technique. Fig. S11 and S12† showed the *Z*-scan data of V measurements of D-**1** and L-**1**, respectively. The TPA absorption coefficient β of D-**1** and L-**1** were calculated as 0.0337 and 0.0279 cm/GW, respectively. Furthermore, the TPA cross section σ was computed as 805 GM for D-**1** and 817 GM for L-**1** (1 GM = 10^{-50} cm^4 s per photon). Ju also reported similar work,[17c] and the 2 PA cross section σ of D-**1** and L-**1** was 392 GM and 389 GM, respectively, which lower than that of this work. Based on this, chiral compound **1** is expected to be applied in the field of nonlinear optics.

Electrochemical measurements

The electrochemical impedance spectroscopy (EIS) measurements and linear sweep voltammogram (LSV) tests of D-**1** and L-**1** were carried out, in order to evaluate their electrochemical enantioselective sensing abilities for chiral substances (D/L-tart molecule). According to the previous literature,[21] a carbon paste working electrode D/L-CPE (D/L-**1** (20 mg) and graphite powder (0.2 g)) was established, and the electrochemical measurement of D/L-cpe was carried out by the conventional three-electrode method. As shown in Fig. 11, the EIS Nyquist plots and LSV curves at different stages were studied on the electrode surface of D-CPE, L-CPE and bare CPE. Obviously, in the mixture of Na_2SO_4 (9 ml, 1 M) and D/L-tart (1 ml, 0.1 M) solutions, the EIS Nyquist plot of D-CPE for D-tart appeared a semicircle at the

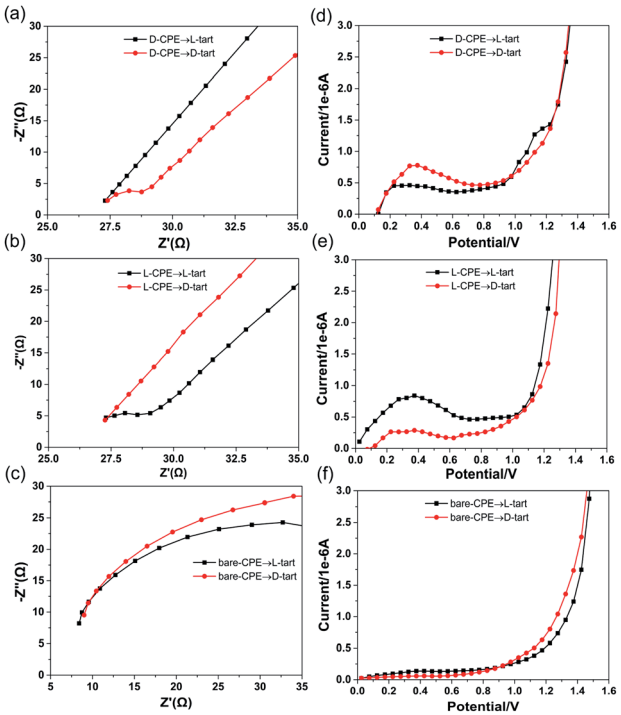

Fig. 11 EIS and LSV of D-CPE (a and d), L-CPE (b and e) and bare CPE (c and f) in the mixture of Na_2SO_4 (9 ml, 1 M) and D/L-tart (1 ml, 0.1 M) solutions at the sweep rate of 100 mV s^{-1} (D-tart and L-tart for red and black line, respectively).

beginning, indicating that an interfacial charge transfer was taking place between D-CPE and Na_2SO_4 solution (Fig. 11a, red line).[22] However, the EIS Nyquist plot of D-CPE for L-tart only showed a straight line in the whole region, demonstrating that only mass diffusion occurred on the D-CPE surface. Beyond that, the same process takes place in the L-CPE system (Fig. 11a, black line). When **l-1** was used as the electrode material, the EIS Nyquist plot of L-CPE for L-tart appeared a semicircle at the beginning, showing that typical interfacial charge transfer was taking place between L-CPE and the mixture of Na_2SO_4 (9 ml, 1 M) and L-tart (1 ml, 0.1 M) solutions (Fig. 11b, black line). While the interfacial electron transfer of L-CPE for D-tart was not observed in the mixture of Na_2SO_4 (9 ml, 1 M) and D-tart (1 ml, 0.1 M) solutions (Fig. 11b, red line).

In order to further prove that chiral compounds have electrochemical enantioselective sensing ability, a blank experiment was carried out. After replacing D-CPE and L-CPE with bare CPE, the EIS Nyquist plots of bare CPE for D- and L-tart only showed straight lines in the whole process (Fig. 11c), which was a typical feature of mass diffusion process, indicating that bare CPE had no enantioselective sensing for D- and L-tart. At the same time, the LSV of **D-1** and **L-1** were also analyzed to fully confirm their enantioselective sensing ability for D/L-tart molecules. In the mixed solution of Na_2SO_4 and D/L-tart, the LSV curve of bare CPE showed that almost no current was generated (Fig. 11f), while the LSV curve of D/L-CPE exhibited peak current in the range of 0–0.6 V (Fig. 11d and e). In addition, the peak current of D-CPE for D-tart is higher than that of L-tart, and the peak current of L-CPE for L-tart is higher than that of D-tart. The result indicates that D-CPE has better enantioselective sensing ability to D-tart, L-CPE has better enantioselective sensing ability to L-tart. However, bare CPE has no selectivity for D- and L-tart molecules.

Taking above discussion into consideration, it can be concluded that the D-CPE possesses enantioselective sensing ability toward the D-tart. Meanwhile, the L-CPE exhibits good enantioselective sensing performance toward the L-tart. LSV tests of D-CPE and L-CPE were consistent with that of impedance experiments, which further corroborate the electrochemical enantioselective sensing abilities of **D-1** and **L-1** for D/L-tart. In addition, By introducing **D-1** or **L-1** into the electrode can also facilitate the electron transfer and promotes enantioselective ability for D/L-tart comparing with the bare CPE.

Conclusions

In summary, in the reaction system of polyoxoanion $[\alpha\text{-}SiW_{11}O_{39}]^{8-}$, copper cations and ethylenediamine ligands by changing the temperatures, compounds **1** and **2** have been designed and synthesized. Samples **1** and **2** are the rare examples of temperature-controlled compounds in the field of POMs, which exhibit as well as good nonlinear optical properties. Moreover, the EIS and LSV measurements have revealed that the D-CPE and L-CPE possess a remarkable enantioselective sensing abilities and electrocatalytic abilities toward D-tart and L-tart, respectively. In light of the success in constructing three compounds, we would not only further synthesize new chiral POMs with spontaneous resolution, but also apply deeper researches to these compounds to develop multifunctional materials.

Conflicts of interest

There are no conflicts to declare.

Acknowledgements

This work was supported by the Natural Science Foundation of China (Grant 21571103) and Jiangsu province (BK20191359) the Major Natural Science Projects of the Jiangsu Higher Education Institution (Grant 16KJA150005).

Notes and references

1 (*a*) A. Dolbecq, E. Dumas, C. R. Mayer and P. Mialane, *Chem. Rev.*, 2010, **110**, 6009–6048; (*b*) Y. Dong, G. Hu, H. Miao, X. He, M. Fang and Y. Xu, *Inorg. Chem.*, 2016, **55**, 11621–11625; (*c*) X.-M. Luo, N.-F. Li, Z.-B. Hu, J.-P. Cao, C.-H. Cui, Q.-F. Lin and Y. Xu, *Inorg. Chem.*, 2019, **58**, 2463–2470.

2 (*a*) S.-S. Wang and G.-Y. Yang, *Chem. Rev.*, 2015, **115**, 4893–4962; (*b*) D.-L. Long, R. Tsunashima and L. Cronin, *Angew. Chem., Int. Ed.*, 2010, **49**, 1736–1758; (*c*) L.-N. Zhang, S.-H. Li, H.-Q. Tan, S. U. Khan, Y.-Y. Ma, H.-Y. Zang, Y.-H. Wang and Y.-G. Li, *ACS Appl. Mater. Interfaces*, 2017, **9**, 16270–16279; (*d*) X. Wei, J. Wei, L. Huang, T. Yan and

F. Luo, *Inorg. Chem. Commun.*, 2017, **81**, 10–14; (*e*) M.-X. Jiang and C.-G. Liu, *J. Phys. Chem. C*, 2017, **121**, 12735–12744.

3 (*a*) M. A. AlDamen, J. M. Clemente-Juan, E. Coronado, C. Martí-Gastaldo and A. Gaita-Arino, *J. Am. Chem. Soc.*, 2008, **130**, 8874–8875; (*b*) U. Kortz, A. Müller, J. van Slageren, J. Schnack, N. S. Dalal and M. Dressel, *Coord. Chem. Rev.*, 2009, **253**, 2315–2327; (*c*) D. Zhang, F. Cao, P. Ma, C. Zhang, Y. Song, Z. Liang, X. Hu, J. Wang and J. Niu, *Chem.–Eur. J.*, 2015, **21**, 17683–17690; (*d*) J. Wang, Y. Niu, M. Zhang, P. Ma, C. Zhang, J. Niu and J. Wang, *Inorg. Chem.*, 2018, **57**, 1796–1805.

4 (*a*) E. Rafiee and S. Shahebrahimi, *J. Mol. Struct.*, 2017, **1139**, 255–263; (*b*) H. Wu, Y.-Q. Zhang, M.-B. Hu, L.-J. Ren, Y. Lin and W. Wang, *Langmuir*, 2017, **33**, 5283–5290.

5 (*a*) A. M. Kaczmarek, K. Van Hecke and R. Van Deun, *Inorg. Chem.*, 2017, **56**, 3190–3200; (*b*) N. Shi, J. Tan, X. Wan, Y. Guan and J. Zhang, *Chem. Commun.*, 2017, **53**, 4390–4393; (*c*) A. Maalaoui, O. Pérez, M. Rzaigui and S. T. Akriche, *J. Alloys Compd.*, 2017, **695**, 1061–1072.

6 D.-Y. Du, L.-K. Yan, Z.-M. Su, S.-L. Li, Y.-Q. Lan and E.-B. Wang, *Coord. Chem. Rev.*, 2013, **257**, 702–717.

7 (*a*) H. Tan, Y. Li, Z. Zhang, C. Qin, X. Wang, E. Wang and Z. Su, *J. Am. Chem. Soc.*, 2007, **129**, 10066–10067; (*b*) F. Xiao, J. Hao, J. Zhang, C. Lv, P. Yin, L. Wang and Y. Wei, *J. Am. Chem. Soc.*, 2010, **132**, 5956–5957; (*c*) J. Zhang, J. Luo, P. Wang, B. Ding, Y. Huang, Z. Zhao, J. Zhang and Y. Wei, *Inorg. Chem.*, 2015, **54**, 2551–2559.

8 (*a*) Y. Wang, L. Shi, Y. Yang, B. Li and L. Wu, *Dalton Trans.*, 2014, **43**, 13178–13186; (*b*) L. Shi, B. Li and L. Wu, *Chem. Commun.*, 2015, **51**, 172–175; (*c*) R. Ishimoto, K. Kamata, K. Suzuki, K. Yamaguchi and N. Mizuno, *Dalton Trans.*, 2015, **44**, 10947–10951; (*d*) Y.-L. Wang, J.-W. Zhao, Z. Zhong, J.-J. Sun, X.-Y. Li, B.-F. Yang and G.-Y. Yang, *Inorg. Chem.*, 2019, **58**, 4657–4664.

9 (*a*) Y. Hou, H. An, T. Xu, S. Zhao and J. Luo, *New J. Chem.*, 2016, **40**, 10316–10324; (*b*) X. Wang, M.-M. Zhang, X.-L. Hao, Y.-H. Wang, Y. Wei, F.-S. Liang, L.-J. Xu and Y.-G. Li, *Cryst. Growth Des.*, 2013, **13**, 3454–3462; (*c*) Z.-M. Zhang, X. Duan, S. Yao, Z. Wang, Z. Lin, Y.-G. Li, L.-S. Long, E.-B. Wang and W. Lin, *Chem. Sci.*, 2016, **7**, 4220–4229.

10 (*a*) P. Cui, L. Ren, Z. Chen, H. Hu, B. Zhao, W. Shi and P. Cheng, *Inorg. Chem.*, 2012, **51**, 2303–2310; (*b*) M. C. Bernini, F. Gandara, M. Iglesias, N. Snejko, E. Gutierrez-Puebla, E. V. Brusau, G. E. Narda and M. A. Monge, *Chem.–Eur. J.*, 2009, **15**, 4896–4905.

11 (*a*) H. An, L. Wang, Y. Hu and F. Fei, *CrystEngComm*, 2015, **17**, 1531–1540; (*b*) H. An, L. Wang, Y. Hu, T. Xu and Y. Hou, *Inorg. Chem.*, 2016, **55**, 144–153.

12 (*a*) Y. Ma, Z. Han, Y. He and L. Yang, *Chem. Commun.*, 2007, 4107–4109; (*b*) C. Zhuo, Y. Wen, S. Hu, T. Sheng, R. Fu, Z. Xue, H. Zhang, H. Li, J. Yuan, X. Chen and X. Wu, *Inorg. Chem.*, 2017, **56**, 6275–6280; (*c*) X.-H. Bu, W. Chen, M. Du, K. Biradha, W.-Z. Wang and R.-H. Zhang, *Inorg. Chem.*, 2002, **41**, 437–439; (*d*) J.-R. Li, Y. Tao, Q. Yu, X.-H. Bu, H. Sakamoto and S. Kitagawa, *Chem.–Eur. J.*, 2008, **14**, 2771–2776.

13 (*a*) I. Katsuki, Y. Motoda, Y. Sunatsuki, N. Matsumoto, T. Nakashima and M. Kojima, *J. Am. Chem. Soc.*, 2002, **124**, 629–640; (*b*) B.-Q. Song, D.-Q. Chen, Z. Ji, J. Tang, X.-L. Wang, H.-Y. Zang and Z.-M. Su, *Chem. Commun.*, 2017, **53**, 1892–1895; (*c*) X.-D. Zheng, M. Zhang, L. Jiang and T.-B. Lu, *Dalton Trans.*, 2012, **41**, 1786–1791; (*d*) X.-L. Tong, T.-L. Hu, J.-P. Zhao, Y.-K. Wang, H. Zhang and X.-H. Bu, *Chem. Commun.*, 2010, **46**, 8543–8545.

14 (*a*) J. Zhang, J. Hao, Y. Wei, F. Xiao, P. Yin and L. Wang, *J. Am. Chem. Soc.*, 2010, **132**, 14–15; (*b*) Y. Hou, X. Fang and C. L. Hill, *Chem.–Eur. J.*, 2007, **13**, 9442–9447; (*c*) S. Liu and X. Qu, *Appl. Surf. Sci.*, 2017, **412**, 189–195.

15 X.-J. Yang, S.-S. Bao, T. Zheng and L.-M. Zheng, *Chem. Commun.*, 2012, **48**, 6565–6567.

16 H. An, Y. Hu, L. Wang, E. Zhou, F. Fei and Z. Su, *Cryst. Growth Des.*, 2015, **15**, 164–175.

17 (*a*) Q. Han, B. Qi, W. Ren, C. He, J. Niu and C. Duan, *Nat. Commun.*, 2015, **6**, 10007; (*b*) Q. Han, C. He, M. Zhao, B. Qi, J. Niu and C. Duan, *J. Am. Chem. Soc.*, 2013, **135**, 10186–10189; (*c*) W.-W. Ju, H.-T. Zhang, X. Xu, Y. Zhang and Y. Xu, *Inorg. Chem.*, 2014, **53**, 3269–3271; (*d*) J. D. Compain, P. Mialane, A. Dolbecq, J. Marrot, A. Proust, K. Nakatani, P. Yu and F. Sécheresse, *Inorg. Chem.*, 2009, **48**, 6222–6228; (*e*) W. Cheng, F.-C. Shen, Y.-S. Xue, X. Luo, M. Fang, Y.-Q. Lan and Y. Xu, *ACS Appl. Energy Mater.*, 2018, **1**, 4931–4938; (*f*) J. Cao, Y. Xiong, X. Luo, L. Chen, J. Shi, M. Zhou and Y. Xu, *Dalton Trans.*, 2018, **47**, 6054–6058; (*g*) J.-P. Cao, Y.-S. Xue, Z.-B. Hu, X.-M. Luo, C.-H. Cui, Y. Song and Y. Xu, *Inorg. Chem.*, 2019, **58**, 2645–2651.

18 A. Téazéa, G. Hervéa, R. G. Finke and D. K. Lyon, *Inorg. Synth.*, 1990, **27**, 85–96.

19 X. He, Y. Liu, Y. Lv, Y. Dong, G. Hu, S. Zhou and Y. Xu, *Inorg. Chem.*, 2016, **55**, 2048–2054.

20 G. Zhang, B. Wang, Y. Wei, Q. Zhang, K. Cai, X. Zhang, Z. Sun and Y. Shi, *Chem. Commun.*, 2016, **69**, 70–74.

21 G. Zhang, H. Hu, H. Li, F. Zhao, Y. Liu, X. He, H. Huang, Y. Xu, Y. Wei and Z. Kang, *CrystEngComm*, 2013, **15**, 3288–3291.

22 (*a*) L. Hu, Y. Sun, Y. Zhou, L. Bai, Y. Zhang, M. Han, H. Huang, Y. Liu and Z. Kang, *Inorg. Chem. Front.*, 2017, **4**, 946–953; (*b*) Y. Zhang, L. Hu, Y. Sun, C. Zhu, R. Li, N. Liu, H. Huang, Y. Liu, C. Huang and Z. Kang, *RSC Adv.*, 2016, **6**, 59956–59960.